AMERICAN ACADEMY OF OPHTHALMOLOGY®

Characteristics and Spatial Distribution of Structural Features in Age-Related Macular Degeneration

A MACUSTAR Study Report

Marlene Saßmannshausen, MD,[1,2] Charlotte Behning, MSc,[3] Jonas Weinz, MSc,[2] Lukas Goerdt, MD,[1,2] Jan H. Terheyden, MD,[1] Petrus Chang, MD,[1,2] Matthias Schmid, PhD,[3] Stephen H. Poor, MRCOphth,[4] Nadia Zakaria, MD, PhD,[5] Robert P. Finger, MD,[1] Frank G. Holz, MD,[1,2] Maximilian Pfau, MD,[1,2,6] Steffen Schmitz-Valckenberg, MD,[1,2,7] Sarah Thiele, MD,[1,2] on behalf of the MACUSTAR consortium members

Purpose: To report the prevalence and topographic distribution of structural characteristics in study participants with age-related macular degeneration (AMD) and controls in the cross-sectional study part of the MACUSTAR study (ClinicalTrials.gov Identifier: NCT03349801).

Design: European, multicenter cohort study.

Subjects: Overall, 301 eyes of 301 subjects with early (n = 34), intermediate (n = 168), and late AMD (n = 43), as well as eyes without any AMD features (n = 56).

Methods: In study eyes with intermediate AMD (iAMD), the presence of structural AMD biomarkers, including pigmentary abnormalities (PAs), pigment epithelium detachment (PED), refractile deposits, reticular pseudodrusen (RPD), hyperreflective foci (HRF), incomplete/complete retinal pigment epithelium (RPE), and outer retinal atrophy (i/cRORA), and quiescent choroidal neovascularization (qCNV) was systematically determined in the prospectively acquired multimodal retinal imaging cross-sectional data set of MACUSTAR. Retinal layer thicknesses and the RPE drusen complex (RPEDC) volume were determined for the total study cohort in spectral-domain (SD) OCT imaging using a deep-learning–based algorithm.

Main Outcome Measures: Prevalence and topographic distribution of structural iAMD features.

Results: A total of 301 study eyes of 301 subjects with a mean (± standard deviation) age of 71.2 ± 7.20 years (63.1% women) were included. Besides large drusen, the most prevalent structural feature in iAMD study eyes were PA (57.1%), followed by HRF (51.8%) and RPD (22.0%). Pigment epithelium detachment lesions were observed in 4.8%, vitelliform lesions in 4.2%, refractile deposits in 3.0%, and qCNV in 2.4%. Direct precursor lesions for manifest retinal atrophy were detected in 10.7% (iRORA) and 4.2% (cRORA) in iAMD eyes. Overall, the highest RPEDC volume with a median of 98.92 × 10^{-4} mm^3 was found in iAMD study eyes. Spatial analysis demonstrated a predominant distribution of RPD in the superior and temporal subfields at a foveal eccentricity of 1.5 to 2 mm, whereas HRF and large drusen had a distinct topographic distribution involving the foveal center.

Conclusions: Detailed knowledge of the prevalence and distribution of structural iAMD biomarkers is vital to identify reliable outcome measure for disease progression. Longitudinal analyses are needed to evaluate their prognostic value for conversion to advanced disease stages.

Financial Disclosure(s): Proprietary or commercial disclosure may be found after the references. *Ophthalmology Retina 2023;■:1–11*

Supplemental material available at www.ophthalmologyretina.org.

Development of advanced disease stages in age-related macular degeneration (AMD), the leading cause of blindness in the elderly population of industrialized countries, is associated with irreversible loss of best-corrected visual acuity (BCVA).[1,2] Although anti-VEGF therapy has revolutionized treatment of patients with exudative AMD, innovative interventions aiming to prevent or decelerate disease progression from early or intermediate AMD (iAMD) to late disease stages are still an unmet need.[3] To test the efficacy of novel drugs in clinical iAMD trials,

https://doi.org/10.1016/j.oret.2022.12.007
ISSN 2468-6530/23

robust and sensitive outcomes measures are needed, allowing for reliable and precise detection and monitoring of disease manifestations and progression.

In recent years, a refined classification of iAMD phenotypes has become possible through multimodal retinal imaging techniques. This includes the detailed assessment of subretinal pigment epithelium (RPE) drusen, reticular pseudodrusen (RPD), refractile deposits, and pigment epithelium detachments (PEDs).[4–6] Besides structural aspects, iAMD phenotyping is also informative of retinal function, e.g., impairment of scotopic retinal sensitivity in the presence of RPD.[7] These diverse phenotypes may be indicative of heterogeneous underlying pathophysiologic pathways.[8,9]

Beyond analyses of retinal layer thicknesses, spectral-domain (SD) OCT allows for a more refined structural assessment of various degenerative alterations. Here, visualization of early photoreceptor degeneration, such as the presence of hyperreflective foci (HRF) or incomplete and complete RPE and outer retinal atrophy (iRORA and cRORA), are assumed to be more sensitive in characterizing early disease progression already in eyes with iAMD and therefore before manifest geographic atrophy (GA).[10]

For the acceptance of such biomarkers as clinical end points by regulators, health care providers, and payers, a comprehensive assessment of structural and coexisting iAMD phenotypes by multimodal imaging and their prevalence within well-designed, large-scale clinical studies is essential.

Therefore, the aim here was to report the prevalence and topographic distribution of structural iAMD biomarkers in the cross-sectional cohort of the MACUSTAR study, a European prospective, multicenter clinical study, and in which standardized and blinded grading of multimodal retinal imaging data was performed in a reader center setting.[11]

Methods

The MACUSTAR Study

The design of the MACUSTAR study (ClinicalTrials.gov Identifier: NCT03349801) has been previously reported in detail.[11,12] In brief, MACUSTAR is a prospective, multicenter, and low-interventional clinical study in subjects with AMD that is conducted at 20 sites in 7 European countries and consists of a cross-sectional and longitudinal study part. Human research ethics committee approval was obtained at all participating clinical sites before enrollment, complying with all applicable legal regulations as previously described.[11] Participants provided informed consent before study recruitment and data collection, and this study has been conducted according to the provisions of the Declaration of Helsinki.

In the MACUSTAR study, subjects were enrolled from March 2018 to February 2020, and the last visit of the last patient is expected for February 2023. Further details on the study protocol and inclusion and exclusion criteria have been recently published elsewhere.[11] For study inclusion, patients had to be aged between 55 and 85 years at baseline visit.[11]

This analysis is based on the cross-sectional study part. Patients had been diagnosed with early, iAMD, or late AMD at baseline visit. Age-similar subjects without any signs of ocular pathology were included as controls. Based on Ferris et al,[13] early AMD was defined as having $\geq$ 1 medium-sized druse (> 63 μm and $\leq$ 125 μm) in the absence of any pigmentary abnormalities (PAs) or signs of iAMD or late AMD in both eyes. Intermediate AMD was defined by large drusen (> 125 μm) and any PA because of AMD present in both eyes. Extrafoveal atrophy outside the central ETDRS subfield of $\leq$ 1.25 mm^2 was permitted in the fellow eye of the iAMD study eye.[11] Patients in the iAMD group also required a BCVA $\geq$ 20/40 Snellen visual acuity equivalent. No macular neovascularization (MNV) was allowed in the fellow eye of iAMD study eyes.

Patients exhibiting bilateral GA ($\geq$ 0.1 mm^2 in fundus autofluorescence [FAF] imaging), bilateral exudative MNV, unilateral GA ($\geq$ 0.1 mm^2), or unilateral MNV with a BCVA between 20/80 and 20/200 Snellen visual equivalent were included in the late AMD group. If both eyes were eligible for any of the study groups based on the specific inclusion criteria, the eye with better visual acuity was selected as the study eye.

Multimodal Retinal Imaging Protocol

Following pupil dilatation with tropicamide 0.5% and phenylephrine 2.5%, patients underwent multimodal retinal imaging according to standard operational procedures by certified study site personnel at screening (V1, day −28 to 0 days), at baseline (V2, day 0) and a validation visit (V3, day 14 ± 7 days). Details on the standardized retinal imaging protocol have been previously reported.[11,14]

In brief, high-speed combined confocal scanning laser ophthalmoscopy and SD-OCT using the Spectralis HRA + OCT device (Heidelberg Engineering, digital imaging resolution 768 × 768 pixels) was acquired. It comprised infrared reflectance (IR, 30° × 30°, automatic real-time mode [ART] mode $\geq$ 30 frames), FAF (30° × 30°, ART mode $\geq$ 30 frames), and SD-OCT imaging (20° × 20°, centered on the fovea, 25 B scans, distance 240 μm, ART mode, 4 frames, and 30° × 25° enhanced−depth-imaging mode, centered on the fovea, 241 B scans, distance between scans 30 μm, ART mode, 9 frames) as well as color fundus photography (CFP). Furthermore, the average corneal curvature for each eye was obtained to enhance the precision of absolute measurements on FAF images.

OCT angiography (OCTA) imaging combined both 3 × 3 mm and 6 × 6 mm cube scans, minimum signal strength 8 (Zeiss Cirrus HD-OCT 5000 Angioplex, Zeiss PLEX Elite 9000 swept-source-OCT) or 20° × 20° and 10° × 10° raster scans (512 B scans with 512 A scans, centered on the fovea, ART 7 mode) performed with the Heidelberg Engineering Spectralis OCT-2 device.

All imaging data were transmitted to the central reading center (GRADE, Reading Center, University of Bonn) through a secure, web-based portal and underwent a quality control review for completeness, technical quality, and adherence to the predefined imaging protocol. If the imaging data were accepted by the data management at the central reading center, retinal imaging data underwent a standardized grading process. Details on the grading strategy of retinal image data are presented in the Supplemental Material (available at www.ophthalmologyretina.org).

Qualitative Grading of Structural Parameters

For the assessment of qualitative structural parameters, a multimodal retinal imaging data approach was applied. Therefore, initially the dense SD-OCT volume raster scan (241 B scans) was considered, whereas additional retinal imaging modalities were referred to depending on the structural parameter as described next.

Besides confirming the study eye's eligibility at the screening visit, baseline multimodal retinal imaging data were graded in eyes with iAMD regarding the presence of pigmentary abnormalities (PAs), PED, refractile deposits, vitelliform lesions, RPD, HRF,

Table 1. Multimodal Retinal Imaging Definition of Structural Biomarkers

Structural Parameter	Multimodal Retinal Imaging Definition	Modality
PA	• Presence of AMD-associated pigmentary changes.[15]	CFP
HRF	• Well-circumscribed, hyperreflective lesions in proximity to drusen with a reflectivity similar to the RPE layer. • Thickness of at least a third of the BM/RPE band. • Detached from the underlying RPE layer.[16,17]	SD-OCT
PED	• RPE elevation with minimum basal diameter of 1000 μm. • Minimum height of 200 μm at the highest point of the elevation measured from the inner edge. of BM to the outer edge of the RPE band.[6]	SD-OCT
Refractile deposits	• Either presence of an intense laminar hyperreflectivity (diameter ≥ 100 μm) at the level of the BM or a pyramidal structure at the level of the outer retina (ghost drusen).[5]	SD-OCT
Vitelliform lesion	• Accumulation of hyperreflective, amorphous material in the subretinal space. • Associated with increased signal in FAF imaging at corresponding location.[18]	SD-OCT, en face 30° FAF
RPD	• Network of oval or roundish irregularities with a variable diameter of ~100 μm in either IR or FAF imaging. • Corresponding to hyperreflective abnormalities/elevations above the RPE/BM with medium-reflective mounds or cones at the level of the ellipsoid zone or between the ellipsoid zone and the RPE surface in SD-OCT imaging.[19,20] • RPD were graded to be present if ≥ 5 individual lesions in > 1 B scan were visible.[21]	En face 30° IR or FAF, SD-OCT
cRORA/iRORA	• Criteria for cRORA presence[22]: (1) region of choroidal hypertransmission of ≥ 250 μm in diameter, (2) zone of attenuation or disruption of the RPE of ≥ 250 μm in diameter, (3) evidence of overlying photoreceptor degeneration, and (4) absence of an RPE tear. • iRORA: presence of aforementioned criteria without fulfilling the size criteria of ≥ 250 μm for cRORA.[23]	SD-OCT
qCNV	• Presence of "double layer sign" or a "shallow irregular RPE elevation" (SIRE) without any signs of exudative activity.[24] • Presence of neovascular network, indicated by a sub-RPE flow signal in OCTA at the corresponding retinal location.[25]	SD-OCT, OCT-A

BM = Bruch's membrane; CFP = color fundus photography; FAF = fundus autofluorescence; HRF = hyperreflective foci; i/cRORA = incomplete/complete retinal pigment epithelium and outer retinal atrophy; OCTA = OCT angiography; PA = pigmentary abnormalities; PED = pigment epithelium detachment; qCNV = quiescent choroidal neovascularization; RPD = reticular pseudodrusen; RPE = retinal pigment epithelium; SD = spectral-domain.

iRORA, cRORA, and quiescent choroidal neovascularization (qCNV). For detailed definitions of structural biomarkers on multimodal retinal imaging see Table 1.[5,6,15–25]

Qualitative assessments of grading parameters were graded as "yes" being present if the graders (both junior and senior) were > 90% sure that a finding is positive. If grading categories were graded as "no," the readers were > 50% sure that the finding was negative. Gradings were determined as "questionable," if the reader suspected a probability of 50% to 90% that a finding was positive. For the following analyses, gradings determined as "questionable" were assigned to the grading category "no."

Quantitative Assessment of Retinal Parameters

Quantitative analysis encompassed the determination of retinal layer thicknesses. Furthermore, the amount and volume of HRF

lesions in the dense SD-OCT volume raster scan, as well as the RPD area in en face 30° IR imaging, were evaluated. Although thicknesses of retinal layers, including the RPE drusen complex (RPEDC) volume, were assessed for the total AMD study cohort (see next), the RPD en face area and quantitative HRF measures were determined only in the iAMD study cohort.

For determination of the RPD area, the IR en face image (30° × 30°) and the reflectivity maps of the retinal layers of inner photoreceptor segments (IS) and outer photoreceptor segments (OS) were extracted from the dense SD-OCT volume raster scan, imported to ImageJ (U.S. National Institutes of Health) and manually aligned to each other according to retinal vessel bifurcations.

After careful consideration of the extracted image data, manual annotation was performed in the en face map with the best delineable en face region of RPD independently by each of the 3 readers (M.S., L.G., S.T.). The final RPD en face area was determined as the mean of the 3 manual annotations.

For each iAMD study patient, each of the 241 SD-OCT B scans was reviewed for the presence of HRF. If present, each single HRF lesion was manually and independently encircled by 2 readers (M.S., L.G.) using the Blow-Lasso Toom in ImageJ on a B-scan level. The topographic coordinates of the annotated HRF lesion within each OCT B scan were used to determine its spatial position and further quantitative measures, like the HRF thickness and volume using Python software; imageio package (Python Software Foundation, version 3.9.5). The HRF volume was calculated based on the annotated HRF area (along the OCT image *x*-axis and the image *y*-axis) being multiplied with the given interscan distance of neighboring B scans (30 μm).

For information on the deep learning-based approach for the SD−OCT-based retinal layer segmentation, please see Supplemental Material.

Topographic analysis of early GA development, iRORA and cRORA lesions were annotated in iAMD study eyes on a B-scan level of the 241 B scans SD-OCT volume scans using a self-developed annotation platform at the GRADE reading center Bonn.

For drusen volume (RPEDC volume) assessment, abnormal RPEDC volumes were defined from the RPEDC thickness of ≥ 3 standard deviations higher than the mean RPEDC thickness of the control group, as previously described in detail.[26,27] Thicknesses for each individual retinal layer as well as RPEDC volumes were quantified in total and for each of the 5 inner subfields (diameter: 3 mm) of the ETDRS grid as well as per AMD disease stage.

Determination of GA Area

In the late AMD group, the area of total GA and of the largest single GA lesion was determined using the Region Finder tool of the Heidelberg Eye Explorer (HEYEX, Heidelberg Engineering) in FAF images as published previously.[28] In accordance with the inclusion criteria for the iAMD group, total GA size was further measured in fellow eyes of the iAMD study group if an extrafoveal total lesion not > 1.25 mm^2 was present.[11]

Statistical Analysis

All statistical analyses were performed using the R software environment (R Foundation, version 4.0.2). The prevalence of structural parameters (e.g., PA, PED, refractile deposits, vitelliform lesions, RPD, HRF, iRORA, cRORA, and qCNV) are given as absolute and relative frequencies within the iAMD subgroup. For the RPD en face area, values were averaged across the gradings of the 3 readers to assess its spatial distribution. Interreader agreement for RPD en face area determination was sufficient (intraclass coefficients 0.958 [95% CI, 0.943−0.969] for Reader (R)1- versus [vs.] -R2; 0.947 [0.929−0.961] for R1- vs. -R3 and 0.945 [0.926−0.959] for R2- vs. -R3). Hyperreflective foci lesions were determined in the central retinal area of 3-mm diameter. Furthermore, their mean number and mean volume of single HRF lesions are presented relative to the 5 inner ETDRS subfields (total 3-mm diameter).

For topographic analysis, RPEDC drusen volumes are given as median values with interquartiles values (q0.25, q0.75), and retinal layer thickness values are presented as mean ± standard deviation for each AMD stage and depending on the corresponding 5 inner ETDRS subfields (3-mm diameter). In addition, boxplots are shown for each AMD stage and ETDRS subfield.

Results

Baseline Characteristics

In the cross-sectional cohort of the MACUSTAR study, a total of 301 eyes of 301 subjects with early (n = 34), iAMD (n = 168), and late AMD (n = 43), as well as eyes without any AMD features (n = 56), were included.

Out of the 43 subjects with late AMD, 12 demonstrated exudative AMD (MNV), whereas the remaining 32 AMD subjects presented with GA in the study eye. One study eye with late-stage AMD had presence of GA and MNV. Mean age of all included subjects was 71.2 years ± 7.20 (standard deviation) with 63.1% being female. Overall BCVA was 0.12 ± 0.30 (mean ± standard deviation) logarithm of the minimum angle of resolution (logMAR), 0.01 ± 0.08 logMAR in the early, 0.02 ± 0.10 logMAR in the intermediate, 0.77 ± 0.25 logMAR in the late AMD, and −0.04 ± 0.08 logMAR in the no-AMD group. For detailed baseline study cohort demographics also see Table 2.

Qualitative Assessment of iAMD Phenotypes

Beyond the presence of large drusen, the highest prevalence of all assessed structural parameters in iAMD eyes (n = 168) was found for PA with 57.1% (n = 96), followed by 51.8% (n = 87) for HRF, and 22.0% (n = 37) for the presence of RPD. In contrast, less frequently observed were PED lesions with a prevalence of 4.8% (n = 8), vitelliform material with 4.2% (n = 7), and refractile deposits with 3.0% (n = 5). With regards to early signs of retinal atrophy development as detected by SD-OCT imaging, the overall prevalence of iRORA lesions was 10.7% (n = 18) compared with 4.2% (n = 7) for cRORA lesions. Topographic analysis revealed a spatial preference of iRORA and cRORA lesions within an eccentricity of 1.5 mm from the foveal center (Fig 1). Evidence for qCNV was found in 2.4% (n = 4) of the iAMD eyes. Detailed results on the prevalence of structural features in iAMD study eyes are shown in Table 3.

Quantitative Assessment of iAMD Phenotypes

Analysis of the RPD En Face Area and Topographic Distribution. In the 37 iAMD eyes with RPD, mean RPD area was 26.0 ± 16.2 mm^2. Reticular pseudodrusen was most frequently detected at an eccentricity of 1.5 to 2 mm superior and temporal to the foveal center. In contrast, RPD was least frequently found in the foveal region (Fig 2A, B).

HRF and Their Topographic Distribution. A total of 87 iAMD eyes (51.8%) had HRF. On a more granular level, a mean of

Table 2. Baseline Study Demographics of the Early, Intermediate, Late AMD, and no-AMD Group as well as of the Total Study Group

	Early AMD (n = 34)	iAMD (n = 168)	Late AMD (n = 43)	No AMD (n = 56)	Overall (n = 301)
Age (yrs)					
Mean ± SD	71.7 ± 6.38	71.2 ± 7.55	74.9 ± 5.59	68.1 ± 6.35	71.2 ± 7.20
Median (Min, max)	72.0 (57.0, 82.0)	72.0 (55.0, 88.0)	75.0 (64.0, 84.0)	68.0 (55.0, 80.0)	72.0 (55.0, 88.0)
Gender					
Female	27 (79.4%)	109 (64.9%)	21 (48.8%)	33 (58.9%)	190 (63.1%)
Male	7 (20.6%)	59 (35.1%)	22 (51.2 %)	23 (41.1%)	111 (36.9%)
Study eyes					
Right	13 (38.2%)	78 (46.4%)	23 (53.5%)	33 (58.9%)	147 (48.8%)
Left	21 (61.8%)	90 (53.6%)	20 (46.5%)	23 (41.1%)	154 (51.2%)
BCVA (logMAR)					
Mean ± SD	0.01 ± 0.08	0.02 ± 0.10	0.77 ± 0.25	−0.04 ± 0.08	0.12 ± 0.30
Median (Min, max)	0.02 (−0.18, 0.20)	0.02 (−0.24, 0.68)	0.84 (0.20, 1.24)	−0.06 (−0.24, 0.14)	0.02 (−0.24, 1.24)

BCVA = best-corrected visual acuity; iAMD = intermediate age-related macular degeneration; logMAR = logarithm of the minimum angle of resolution; SD = standard deviation.

14.0 ± 26.12 single HRF lesions were detected in iAMD (n = 168) study eyes.

Spatial assessment revealed that single-lesion HRF were most likely found in the central ETDRS subfield (mean ± standard deviation; 4.14 ± 10.70) in contrast to the perifoveal subfields (nasal inner, 2.0 ± 5.55; inferior inner, 1.95 ± 6.0; temporal inner, 1.82 ± 5.2; and superior inner, 1.44 ± 4.4).

Overall mean thickness of HRF lesions was 17.52 ± 8.69 μm. Furthermore, quantitative assessment of HRF volume showed that the largest values ($826.84 \times 10^2 \pm 1107.9 \times 10^2$ μm^3) were found in the central ETDRS subfield. Median HRF single-lesion volume within the 4 paracentral inner ETDRS subfields was 23 952.48 μm^3, range $1600.52 - 6688.01 \times 10^2$ μm^3. A graphical en face illustration of the topographic HRF lesion distribution is presented in Figure 3.

RPEDC Volume and Retinal Layer Thickness Analysis. The thickness of retinal layers and the RPEDC volume were quantitatively determined in the dense (241 B scans) SD-OCT volume raster scan. Overall, 167 out of 168 iAMD subjects were assessed for quantitative retina layer analysis, with one iAMD subject excluded because of insufficient image quality. No SD-OCT image data from the other study groups were excluded because of image quality.

The greatest RPEDC volume was found in the iAMD group with a median (q0.25, q0.75) volume of 98.92 (10.35, 514.92) $\times 10^{-4}$ mm^3, followed by 48.52 (9.12, 220.22) $\times 10^{-4}$ mm^3 in the late, 0.01 (0.00, 0.19) $\times 10^{-4}$ mm^3 in the early and 0.001 (0.00, 0.01) $\times 10^{-4}$ mm^3 in the no-AMD study group. Considering topography, the highest RPEDC volume was detected in the central subfield of the iAMD study group with a median volume of 9.93 (0.04, 79.76) $\times 10^{-4}$ mm^3. Regarding RPEDC volumes within the inner ETDRS subfields of the iAMD group, an overall highest RPEDC volume was found in the inferior inner subfield with 16.20 (0.32, 97.60) $\times 10^{-4}$ mm^3, whereas the lowest RPEDC volume was observed in the nasal inner subfield with 8.48 (0.19, 67.66) $\times 10^{-4}$ mm^3. For a graphical illustration of the topographic distribution of RPEDC volumes within all assessed AMD groups relative to EDTRS subfields, see Figure 4.

The highest RPD presence in iAMD eyes is associated with a smaller RPEDC volume in the central subfield with a median (q0.25, q0.75) volume with RPD of 4.04 (0.11, 25.47) $\times 10^{-4}$ mm^3, and a median volume without RPD of 11.71 (0.04, 109.51) $\times 10^{-4}$ mm^3 (Fig 4B). Retinal layer analysis revealed a mean total retinal thickness of 331.54 ± 17.36 μm in the early, 333.47 ± 21.98 μm in the intermediate, 244.74 ± 63.32 μm in the late AMD, and of 331.70 ± 13.22 μm in the no-AMD study group. More relevant to AMD disease alterations, we found the total outer retinal thickness, i.e., including the outer nuclear layer (ONL), the OS, and IS layer, was 122.29 ± 9.58 μm in the early, 118.62 ± 27.00 μm in the intermediate, and 52.93 ± 44.15 μm in the late AMD group. In comparison, the no-AMD group showed a mean thickness of 123.72 ± 7.10 μm.

Mean GCL thickness was 43.84 ± 4.93 μm in the early, 42.63 ± 5.60 μm in the intermediate, 38.64 ± 8.31 μm in the late AMD, and 43.58 ± 4.76 μm in the no-AMD group. Detailed results of the comprehensive analysis of RPEDC volume, including median and interquartile values for all study groups and for iAMD study eyes without RPD as well as results of various retinal layers for the study subgroups, total and individual ETDRS subfields (diameter 3 mm) are presented in Figure S5 and Tables S4, S5, and S6 (available at www.ophthalmologyretina.org).

Presence of GA. Of the 168 eyes of 168 included iAMD subjects, 6 (3.6%) participants had extrafoveal GA in the fellow eye with a mean area of 0.3 ± 0.2 mm^2 (Table 3). Out of the 43 subjects with late AMD, GA was present in 32 (74.4%) study eyes with a mean area of 11.9 ± 9.3 mm^2 as assessed by FAF image analysis. Multifocal GA lesions were present in 30 eyes (69.7%) with a mean of 2.9 ± 2.2 lesions per eye. The mean area of the largest single lesion was 10.7 ± 9.3 mm^2. Detailed results on the late AMD study group are given in Table 7.

Discussion

In this study, qualitative and quantitative characteristics of structural biomarkers as well as their spatial distribution across different AMD disease stages were analyzed within a multimodal, prospectively acquired retinal image data set from the cross-sectional part of the MACUSTAR study. Furthermore, an innovative image analysis approach, i.e., a

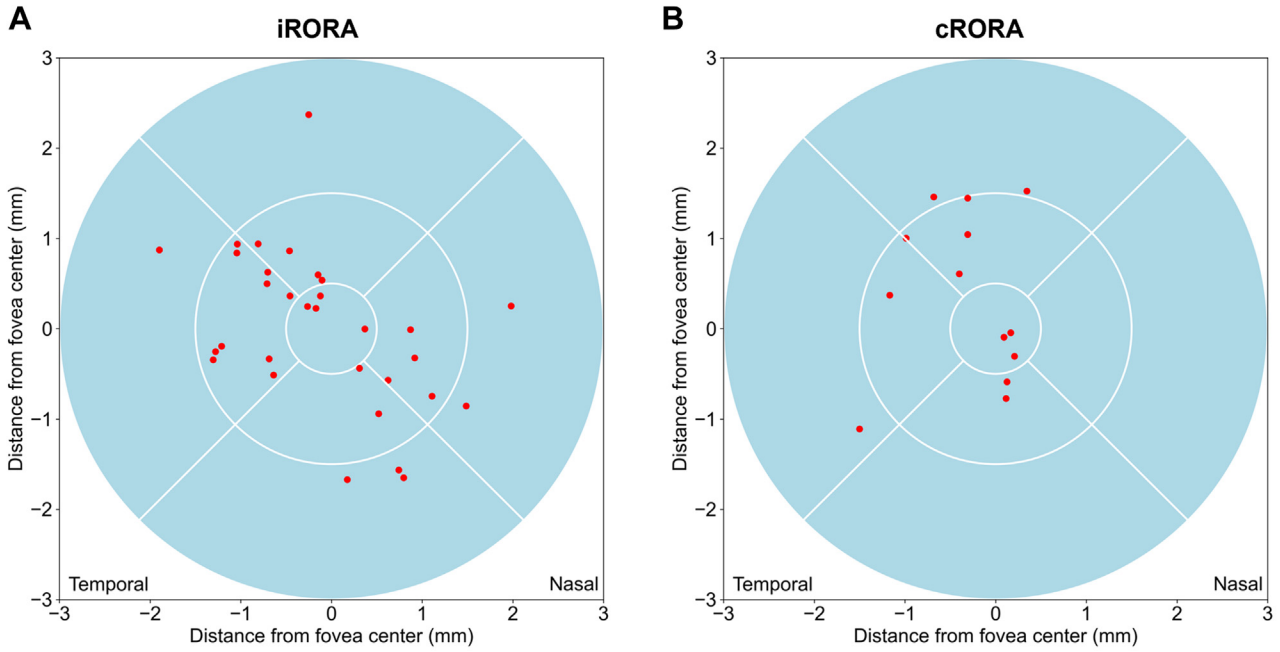

Figure 1. Topographic distribution of iRORA and cRORA lesions in iAMD study eyes. The plots show the location of iRORA and cRORA lesions relative to the ETDRS study grid (diameter 6 mm). Red dots indicate the exact en face position of each lesion of iRORA, and cRORA detected in iAMD study eyes (n = 18 with iRORA and n = 7 with cRORA). iRORA = Incomplete retinal pigment epithelium and outer retinal atrophy; i/cRORA = incomplete/complete retinal pigment epithelium and outer retinal atrophy; iAMD = intermediate age-related macular degeneration.

deep-learning-based algorithm, was applied to allow reliable thickness determination of retinal layers and RPEDC volume in SD-OCT imaging. Within iAMD study eyes, the highest prevalence rates were determined for presence of PA, HRF, and RPD, whereas further analysis indicated a topographic association between the presence of large drusen, HRF, and iRORA lesions.

Table 3. Qualitative Assessment of Structural Parameters in iAMD Study Eyes and for Extrafoveal GA Assessment in the Fellow Eyes

Structural Parameter in the Study Eye	iAMD (n = 168)
Pigmentary abnormalities, n (%)	96 (57.1)
HRF, n (%)	87 (51.8)
PED lesions, n (%)	8 (4.8)
Refractile deposits, n (%)	5 (3.0)
Vitelliform material, n (%)	7 (4.2)
RPD, n (%)	37 (22.0)
iRORA, n (%)	18 (10.7)
cRORA, n (%)	7 (4.2)
qCNV, n (%)	4 (2.4)
Extrafoveal GA determination in the fellow eye	
Number of eyes, n (%)	6 (3.6)
Mean (± SD) **GA lesion size** (mm^2)	0.3 ± 0.2
Median (Min; max) **GA lesion size** (mm^2)	0.2 (0.1–0.3)

cRORA = complete retinal pigment epithelium and outer retinal atrophy; GA = geographic atrophy; HRF = hyperreflective foci; iRORA = incomplete retinal pigment epithelium and outer retinal atrophy; iAMD = intermediate age-related macular degeneration; PED = pigment epithelium detachment; qCNV = quiescent choroidal neovascularization; RPD = reticular pseudodrusen.

Qualitative analysis showed PA, as assessed by CFP imaging, to be the most common feature (prevalence 57.1%) in iAMD eyes besides the presence of large drusen, which are both features defining intermediate disease stage following the Beckman classification.[13] In the context of another iAMD trial (the LEAD trial), Guymer et al[29] reported a PA prevalence of 31.3% in AMD subjects with bilateral large drusen at baseline. A possible explanation for the difference in PA prevalence rates is different inclusion criteria. In the LEAD trial, early outer retinal atrophy (i.e., nascent GA) in either eye was an exclusion criteria, whereas such lesions were allowed in MACUSTAR and were present in approximately 15% of patients. Furthermore, study patients with iAMD in the cross-sectional MACUSTAR study were allowed with extrafoveal GA ($\leq$ 1.25 mm^2) in the fellow eye and were present in 3.6% of patients. The more advanced degenerative alterations within in the MACUSTAR study are assumed to impact the higher PA prevalence. Interestingly, 76.1% of 314 iAMD study patients in the Age-Related Eye Disease Study 2 (AREDS2) trial were reported to exhibit hyperpigmentary changes on CFP imaging.[30] Given extrafoveal GA lesions were permitted in iAMD AREDS2 study eyes, the AREDS2 iAMD cohort may have had more advanced disease than the MACUSTAR cohort,[31] which likely had a slightly higher disease burden than participants in the LEAD study.

Hyperreflective foci is currently assumed to be structural SD-OCT surrogates for CFP-based PA.[30,32] Although the

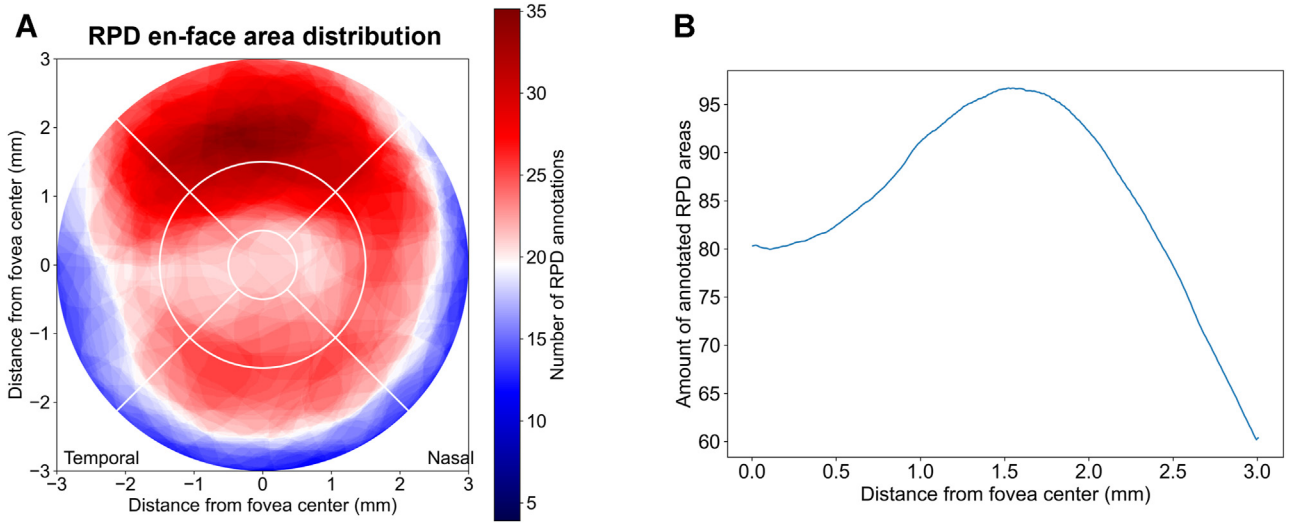

Figure 2. Topography of RPD. This figure provides a graphical heat-map presentation (**A**) and eccentricity analysis (**B**) of the topographic distribution of annotated RPD en face areas in iAMD study eyes (n = 37) relative to the ETDRS study grid (diameter 6 mm). The topographic heat-map (**A**) illustrates the predominant localization of annotated RPD areas in an epicenter superior to the fovea with a peak presence at an eccentricity of 1.5 to 2 mm from the foveal center point (**B**). RPD = reticular pseudodrusen; iAMD = intermediate age-related macular degeneration.

HRF prevalence (51.8%) was comparable with the reported PA prevalence of 57.1%, HRF was less frequently detected than PA in iAMD participants of the cross-sectional MACUSTAR study. This finding is in line with results by Folgar et al,[30] who reported from a subgroup analysis of iAMD eyes of the AREDS2 trial that CFP-based PA were spatially matched in only 71.8% of HRF lesions on SD-OCT imaging. In this context, Folgar et al[30] further demonstrated that PA in CFP imaging, and in particular hyperpigmentary changes, might also be present because of RPE hypertrophy, hyperpigmentation of the choroid, and sub-RPE space that have not yet manifest as HRF in SD-OCT.[30] Because the distance of neighboring B scans in the dense volume raster scan (30° × 25° scan field with 241 B scans) is approximately 30 µm, smaller HRF lesions might inevitably be missed during image acquisition potentially explaining the discordant HRF vs. PA prevalence rates.

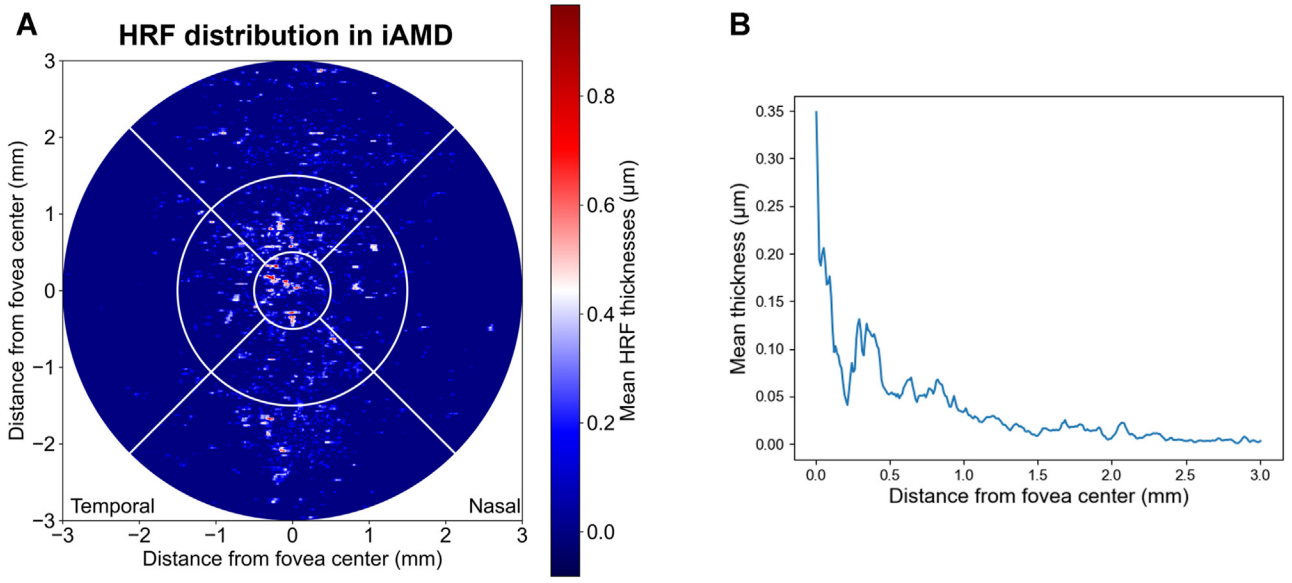

Figure 3. Graphical heat-map presentation (**A**) and eccentricity analysis (**B**) of the topographic HRF distribution in iAMD study eyes relative to ETDRS study grid (diameter 6 mm). Mean thickness (µm) of each HRF lesion was assessed for color-coded graphical en face illustration of HRF distribution (**A**). Eccentricity analysis (**B**) revealed HRF lesions were predominantly detected within 1 mm of the central retinal region (n = 87). HRF = hyperreflective foci; iAMD = intermediate age-related macular degeneration.

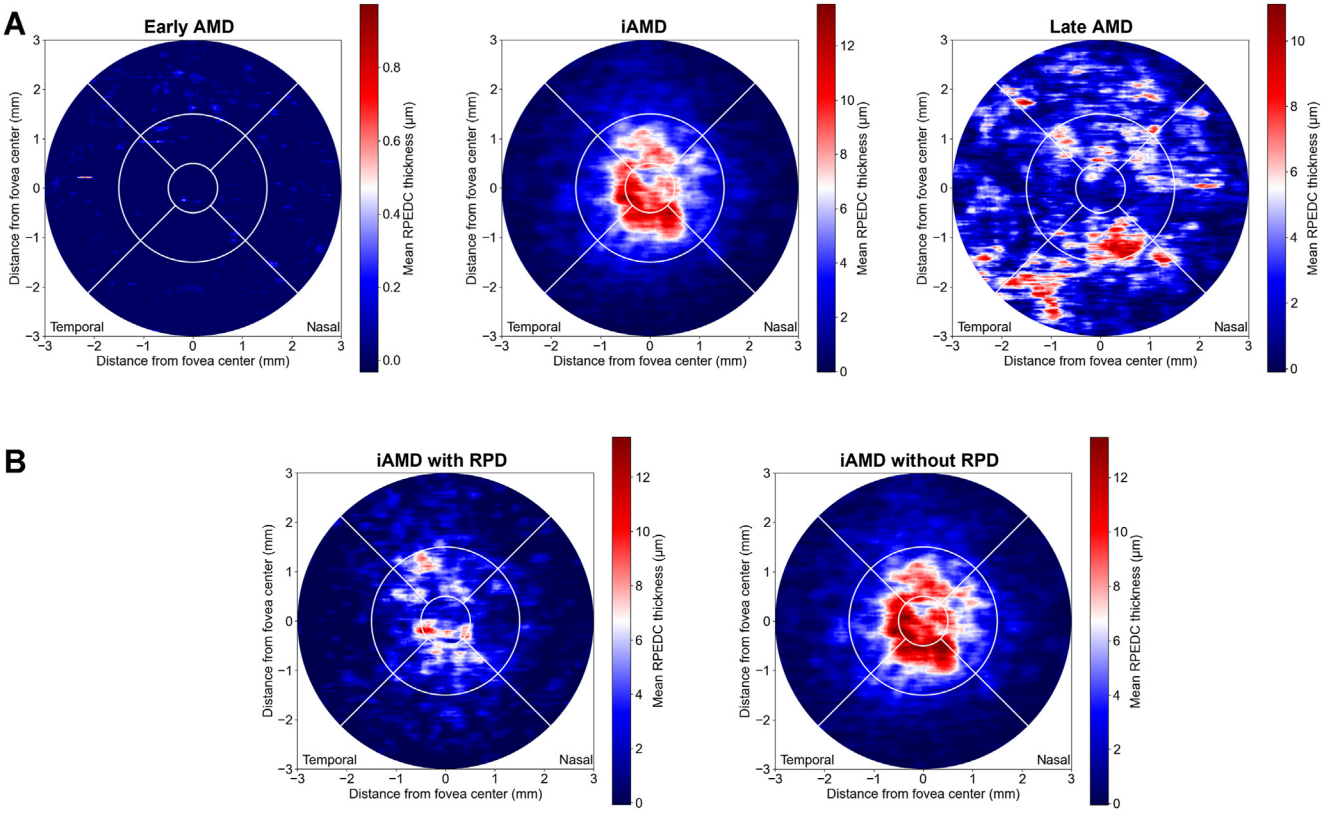

Figure 4. Heat-map illustration of the topographic distribution of drusen in terms of the mean RPEDC thickness within all AMD study groups (**A**) as well as in iAMD study eyes with and without RPD (**B**) relative to ETDRS study grid (diameter 6 mm). Note, the greatest drusen load, as determined by RPEDC volume, was found in iAMD study eyes. The mean RPEDC thickness (µm) was assessed for the color-coded graphical en face illustration of drusen load. REPDC = Retinal Pigment Epithelium Drusen Complex; iAMD = intermediate age-related macular degeneration; RPD = reticular pseudodrusen.

Another established iAMD high-risk feature for disease progression is RPD, which were present in 22.0% of iAMD study eyes. Despite different approaches to RPD grading and potentially different stages of disease, the prevalence of RPD in MACUSTAR aligns well with the 23.8% and 26.0% prevalence reported in the LEAD and AREDS2 trials, respectively.[29,33] Moreover, the observed spatial pattern of RPD reported here is well aligned with previous reports of the spatial progression of RPD (cf., Fig 2).[4,34,35] A previously reported higher prevalence rate of 44% in iAMD eyes is likely related to a majority of subjects with advanced AMD (either central GA or CNV) in the fellow eye.[36]

Table 7. Qualitative and Quantitative Assessment of Structural Parameters in the Late AMD Study Group

Structural Parameter in the Study Eye	Late AMD (n = 43)
Evidence of exudation, n (%)	12 (27.91%)
Evidence of GA, n (%)	32 (74.4%)
Total GA size (in mm^2)	
Mean ± SD	11.9 ± 9.3
Median (Min; max)	9.4 (0.89–32.91)
Largest single GA lesion size (in mm^2)	
Mean ± SD	10.7 ± 9.3
Median (Min; max)	7.6 (0.85–32.91)
Total number of atrophy lesions	
Mean ± SD	2.9 ± 2.2
Median (Min; max)	2.0 (1.0–3.8)
Foveal involvement of GA, n (%)	27 (62.79)
Presence of diffuse trickling phenotype, n (%)	4 (9.3)

AMD = age-related macular degeneration; GA = geographic atrophy; SD = standard deviation.

A structural measure for drusen load in 3-dimensional SD-OCT imaging is RPEDC volume.[26,27,37,38] As expected across all AMD stages, the greatest RPEDC volume was found in the iAMD study group (0.04 ± 0.07 mm^3). The AREDS2 study reports a similar volume of OCT drusen load in iAMD eyes (0.08 ± 0.16 mm^3).[26] However, a direct comparison of values for 3-dimensional drusen load are challenging because different OCT devices and retinal areas (3- vs. 5-mm diameter) were assessed.[26] Furthermore, the presented results of topographic drusen analysis are in accordance with previous findings of both histologic and clinical studies.[37,38] Visual assessment of heat-map representation for HRF (Fig 3) and drusen (Fig 4) topography in the MACUSTAR study indicates a spatial correlation of drusen load and HRF consistent with recent findings by Waldstein et al.[37]

Although these biomarkers have prognostic relevance for AMD progression, refining and identifying more sensitive

biomarkers and outcome measures in merging clinical trials would be prudent. In particular, high-resolution retinal imaging has aided identification of precursor lesions for manifest GA.[22,39,23] Recently, in a case series of 72 iAMD eyes, Jhingan et al[40] detected iRORA 11% and cRORA in 5.5% of cases. Although these prevalence data were derived from a single-center study, MACUSTAR results on the presence of iRORA (10.7%) and cRORA (4.2%) are comparable. In addition, and for the first time, this study report outlines the topography of iRORA and cRORA development (Fig 1), which indicates in visual assessment a spatial correlation with the topography of HRF and drusen load (cp. Figs 3, 4).

Several limitations need to be discussed. First, this analysis was performed on a cross-sectional data set of the MACUSTAR study, which therefore impedes determination of any biomarkers' prognostic value regarding conversion into late AMD stages. Second, only structural image data have been assessed in this study. However, given the unique and manifold MACUSTAR data set, which also includes spatially resolved functional data as well as data on the genetic risk profiles, studies on a more refined characterization and identification of innovative (composite-) end points are already ongoing.

In this context, clinical-histopathologic correlation is also needed to better understand the nature and clinical relevance of structural biomarkers, similar to HRF lesions, on a more granular level. Here, it also needs to be considered that, given the nature of OCT volume raster scanning, it might not always be possible to differentiate between single or clustered HRF lesions in neighboring OCT B scans.

Finally, it needs to be stated that the MACUSTAR study groups were classified according to the well-established AMD classification system by the Beckman consortium, which is primarily based on CFP assessment and does not comprehend more recently highlighted structural iAMD features, similar to RPD, quiescent MNV, and iRORA/cRORA lesions. Again, multimodal imaging studies similar to MACUSTAR are here demanded to provide more knowledge on their clinical relevance within the pathophysiologic spectrum of AMD.

In conclusion, the structural baseline characteristics of the cross-sectional MACUSTAR study cohort are similar to other recent iAMD trials (e.g., LEAD). The analysis of biomarkers' topography revealed a spatial association in particular of large drusen, HRF, and early lesions of photoreceptor degeneration, i.e., iRORA/cRORA. Because these were revealed to be most frequently prevalent in the perifoveal area, this study further supports the need for identification of novel iAMD biomarkers, which might serve, apart from the assessment of the BCVA and therefore foveolar integrity, as sensitive outcome measures in future iAMD trials. Analyses of the longitudinal MACUSTAR data set will provide an understanding of progression to advanced AMD stages. The unique data set of MACUSTAR, comprising data on retinal functional, patients' reported outcome measures, and genetic factors, have the opportunity to identify innovative (and compound) end points and analyses of the longitudinal data set are now warranted to better understand both their clinical relevance and prognostic value for disease progression.

Footnotes and Disclosures

Originally received: August 12, 2022.
Final revision: November 13, 2022.
Accepted: December 13, 2022.
Available online: ■■■. Manuscript no. ORET-D-22-00516R1

[1] Department of Ophthalmology, University Hospital Bonn, Bonn, Germany.

[2] GRADE Reading Center, University of Bonn, Bonn, Germany.

[3] Institute of Medical Biometry, Informatics and Epidemiology, University Hospital Bonn, Bonn, Germany.

[4] Ophthalmology Research, Novartis Institutes for Biomedical Research, Cambridge, Massachusetts.

[5] Ophthalmology Translational Medicine, Novartis Institutes for Biomedical Research, Cambridge, Massachusetts.

[6] Institute of Molecular and Clinical Ophthalmology Basel, Basel, Switzerland.

[7] John A. Moran Eye Center, Department of Ophthalmology & Visual Sciences, University of Utah, Salt Lake City, Utah.

Disclosures:

All authors have completed and submitted the ICMJE disclosures form.

The authors have made the following disclosures:

M.S.: Grant − BONFOR GEROK Program, Faculty of Medicine, University of Bonn (grant no.: O-137.0030), Anna-Katharina Eichenauer Foundation; Funding − Heidelberg Engineering, CenterVue, Carl Zeiss MedicTec.

J.W.: Employee − GRADE Reading Center.

L.G.: Payment − Novartis; Support − ARVO.

J.H.T.: Funding − Innovative Medicines Initiative (IMI2 Program), Heidelberg Engineering, Optos, Zeiss, CenterVue; Payment − Novartis, Okko.

S. P.: Employee − Novartis; Stocks − Novartis.

N.Z.: Employee − Novartis; Stocks − Novartis.

R.P.F.: Support − Bayer, Carl Zeiss MediTec, Novartis, Roche; Grants − Biogen; Consultant − Bayer, Alimera, Apellis, Allergan, Biogeŋ Novartis, Roche/Genentech, Böhringer-Ingelheim, OD-OS, Opthea, ProQR; Honoraria − Apellis, Novartis, Alimera, Chiesi.

F.G.H.: Grants − Bayer, Carl Zeiss MediTec, Novartis, Roche. Contracts − NightStar, Katairo, Kubota Vision, Pixium, Optos, Apellis, Allergan, Bioeq/Formycon, Novartis, Roche/Genentech, Heidelberg Engineering; Consultant − Alzheon, Oxurion, Allergan, Apellis, Bioeq/Formycon, Novartis, Roche/Genentech, IvericBio, Geuder, Annexon, Astellas, Complement Therapeutics; Honoraria − Apellis, Heidelberg Engineering, Bayer; Executive Board Member − Euretina, Club Jules Gonin, German Ophthalmological Society; Co-founder − STZ GRADE Reading Center.

M.P.: Grant − German Research Foundation (DFG); Consultant − Apellis Pharmaceuticals; Honoraria − Apellis Pharmaceuticals, Novartis.

S.S.-V.: Grants − Bayer, Carl Zeiss MediTec, Novartis, Roche; Contract − AlphaRet, Katairo, Kubota Vision, Pixium, SparingVision, Apellis, Allergan, Bioeq/Formycon, Novartis, Roche/Genentech, Heidelberg Engineering; Consultant − Galimedix, Oxurion, Apellis, Allergan, Bioeq/Formycon, Novartis, Roche/Genentech; Honoraria − Apellis, Heidelberg Engineering; Co-founder − STZ GRADE Reading Center.

S.T.: Grant − German Research Foundation (grant no.: DFG, TH 2514/2-1), Maria-von-Linden Program, University of Bonn, Bonfor Research Grant, Dr. Werner Jackstädt Nachwuchspreis of the German Retina Society, Young researcher grant (Anschubfinanzierung) provided by the German Society of Ophthalmology (DOG); Payment − Heidelberg Engineering, Novartis, Bayer, Allergan; Participation − Novartis; Other financial or non-financial interests − Heidelberg Engineering; Optos, Zeiss, CenterVue.

The other authors have no proprietary or commercial interest in any materials discussed in this article.

Supported by the Innovative Medicines Initiative (IMI) 2 Joint Undertaking under grant agreement No. 116076. This Joint Undertaking receives support from the European Union's Horizon 2020 research and innovation programme and the European Federation of Pharmaceutical Industries and Associations (EFPIA).

HUMAN SUBJECTS: Human subjects were included in this study.

All institutional ethic committees approved the study and participants gave written informed consent before participation. These committees included University Hospital Bonn ethics committee (384/17), Paris Ouest IV (04/18_2), AIBILI (032/2017/AIBILI/CE), Nova Medical School (13507/2017), London Queen Square Research Ethics Committee (18/LO/0145), Center for Sundhed Glostrup (H-18000126), Comitato Etico Milano (37910/2018), Ospedale San Raffaele (dated 25/10/2018), Radboudumc technology center (2017−3954) and LUMC commissie medische ethiek (L18.055/SH/sh).

No animal subjects were used in this study.

Author Contributions:

Conception and design: Saßmannshausen, Behning, Terheyden, Chang, Schmid, Poor, Zakaria, Finger, Holz, Pfau, Schmitz-Valckenberg, Thiele.

Analysis and interpretation: Saßmannshausen, Behning, Weinz, Goerdt, Terhenyden, Schmid, Finger, Holz, Pfau, Schmitz-Valckenberg, Thiele.

Data collection: Saßmannshausen, Behning, Terheyden, Chang, Schmid, Finger, Holz, Pfau, Schmitz-Valckenberg, Thiele.

Obtained funding: N/A; The sponsor or funding organization had no role in the design or conduct of this research.

Overall responsibility: Saßmannshausen, Behning, Weinz, Goerdt, Terhenyden, Chang, Poor, Zakaria, Schmid, Finger, Holz, Pfau, Schmitz-Valckenberg, Thiele.

Abbreviations and Acronyms:
AMD = age-related macular degeneration; **ART** = automatic real-time mode; **BCVA** = best-corrected visual acuity; **CFP** = color fundus photography; **CNV** = choroidal neovascularization; **HRF** = hyperreflective foci; **i/cRORA** = incomplete/complete retinal pigment epithelium and outer retinal atrophy; **logMAR** = logarithm of the minimum angle of resolution; **qCNV** = quiescent choroidal neovascularization; **IR** = infrared reflectance; **MNV** = macular neovascularization; **PA** = pigmentary abnormalities; **PED** = pigment epithelium detachment; **RPD** = reticular pseudodrusen; **RPE** = retinal pigment epithelium; **RPEDC** = retinal pigment epithelium drusen complex; **SD** = spectral-domain; **vs** = versus.

Keywords:
Age-related macular degeneration, Biomarker, Intermediate age-related macular degeneration, Phenotyping.

Correspondence:
Sarah Thiele, MD, Venusberg-Campus 1,53127 Bonn, Germany. E-mail: sarah.thiele@ukbonn.de.

References

1. Wong WL, Su X, Li X, et al. Global prevalence of age-related macular degeneration and disease burden projection for 2020 and 2040: a systematic review and meta-analysis. *Lancet Glob Health*. 2014;2:e106−e116.
2. Lim LS, Mitchell P, Seddon JM, et al. Age-related macular degeneration. *Lancet*. 2012;379:1728−1738.
3. Fleckenstein M, Keenan TDL, Guymer RH, et al. Age-related macular degeneration. *Nat Rev Dis Primers*. 2021;7:31.
4. Wu Z, Fletcher EL, Kumar H, et al. Reticular pseudodrusen: a critical phenotype in age-related macular degeneration. *Prog Retin Eye Res*. 2022;88:101017.
5. Suzuki M, Curcio CA, Mullins RF, Spaide RF. Refractile drusen: clinical imaging and candidate histology. *Retina*. 2015;35:859−865.
6. Tan ACS, Simhaee D, Balaratnasingam C, et al. A perspective on the nature and frequency of pigment epithelial detachments. *Am J Ophthalmol*. 2016;172:13−27.
7. Zhang Y, Sadda SR, Sarraf D, et al. Spatial dissociation of subretinal drusenoid deposits and impaired scotopic and mesopic sensitivity in AMD. *Invest Ophthalmol Vis Sci*. 2022;63:32.
8. Spaide RF. Outer retinal atrophy after regression of subretinal drusenoid deposits as a newly recognized form of late age-related macular degeneration. *Retina*. 2013;33:1800−1808.
9. Rogala J, Zangerl B, Assaad N, et al. In vivo quantification of retinal changes associated with drusen in age-related macular degeneration. *Invest Ophthalmol Vis Sci*. 2015;56:1689−1700.
10. Christenbury JG, Folgar FA, O'Connell RV, et al. Progression of intermediate age-related macular degeneration with proliferation and inner retinal migration of hyperreflective foci. *Ophthalmology*. 2013;120:1038−1045.
11. Terheyden JH, Holz FG, Schmitz-Valckenberg S, et al. Clinical study protocol for a low-interventional study in intermediate age-related macular degeneration developing novel clinical endpoints for interventional clinical trials with a regulatory and patient access intention-MACUSTAR. *Trials*. 2020;21:659.
12. Finger RP, Schmitz-Valckenberg S, Schmid M, et al. MACUSTAR: development and clinical validation of functional, structural, and patient-reported endpoints in intermediate age-related macular degeneration. *Ophthalmologica*. 2019;241:61−72.
13. Ferris FL, Wilkinson CP, Bird A, et al. Clinical classification of age-related macular degeneration. *Ophthalmology*. 2013;120:844−851.
14. Saßmannshausen M, Thiele S, Behning C, et al. Intersession repeatability of structural biomarkers in early and intermediate age-related macular degeneration: a MACUSTAR study report. *Trans Vis Sci Technol*. 2022;11:27.
15. Thiele S, Pfau M, Larsen PP, et al. Multimodal imaging patterns for development of central atrophy secondary to age-related macular degeneration. *Invest Ophthalmol Vis Sci*. 2018;59:AMD1−AMD11.
16. Jaffe GJ, Chakravarthy U, Freund KB, et al. Imaging features associated with progression to geographic atrophy in age-related macular degeneration: classification of atrophy meeting report 5. *Ophthalmol Retina*. 2021;5:855−867.
17. Curcio CA, Zanzottera EC, Ach T, Balaratnasingam C, Freund KB. Activated retinal pigment epithelium, an optical coherence tomography biomarker for progression in age-related macular degeneration. *Invest Ophthalmol Vis Sci*. 2017;58:BIO211−BIO226.

18. Balaratnasingam C, Hoang QV, Inoue M, et al. Clinical characteristics, choroidal neovascularization, and predictors of visual outcomes in acquired vitelliform lesions. *Am J Ophthalmol*. 2016;172:28–38.
19. Querques G, Querques L, Martinelli D, et al. Pathologic insights from integrated imaging of reticular pseudodrusen in age-related macular degeneration. *Retina*. 2011;31:518–526.
20. Spaide RF, Curcio CA. Drusen characterization with multimodal imaging. *Retina*. 2010;30:1441–1454.
21. Zweifel SA, Imamura Y, Spaide TC, et al. Prevalence and significance of subretinal drusenoid deposits (reticular pseudodrusen) in age-related macular degeneration. *Ophthalmology*. 2010;117:1775–1781.
22. Sadda SR, Guymer R, Holz FG, et al. Consensus definition for atrophy associated with age-related macular degeneration on OCT: classification of atrophy report 3. *Ophthalmology*. 2018;125:537–548.
23. Guymer RH, Rosenfeld PJ, Curcio CA, et al. Incomplete retinal pigment epithelial and outer retinal atrophy in age-related macular degeneration: classification of atrophy meeting report 4. *Ophthalmology*. 2020;127:394–409.
24. Narita C, Wu Z, Rosenfeld PJ, et al. Structural OCT signs suggestive of subclinical nonexudative macular neovascularization in eyes with large drusen. *Ophthalmology*. 2020;127:637–647.
25. de Carlo TE, Bonini Filho MA, Chin AT, et al. Spectral-domain optical coherence tomography angiography of choroidal neovascularization. *Ophthalmology*. 2015;122:1228–1238.
26. Folgar FA, Yuan EL, Sevilla MB, et al. Drusen volume and retinal pigment epithelium abnormal thinning volume predict 2-year progression of age-related macular degeneration. *Ophthalmology*. 2016;123:39–50.e1.
27. Farsiu S, Chiu SJ, O'Connell RV, et al. Quantitative classification of eyes with and without intermediate age-related macular degeneration using optical coherence tomography. *Ophthalmology*. 2014;121:162–172.
28. Schmitz-Valckenberg S, Brinkmann CK, Alten F, et al. Semiautomated image processing method for identification and quantification of geographic atrophy in age-related macular degeneration. *Invest Ophthalmol Vis Sci*. 2011;52:7640–7646.
29. Guymer RH, Wu Z, Hodgson LAB, et al. Subthreshold nanosecond laser intervention in age-related macular degeneration: the LEAD randomized controlled clinical trial. *Ophthalmology*. 2019;126:829–838.
30. Folgar FA, Chow JH, Farsiu S, et al. Spatial correlation between hyperpigmentary changes on color fundus photography and hyperreflective foci on SDOCT in intermediate AMD. *Invest Ophthalmol Vis Sci*. 2012;53:4626–4633.
31. Chew EY, Clemons T, SanGiovanni JP, et al. The age-related eye disease study 2 (AREDS2): study design and baseline characteristics (AREDS2 report number 1). *Ophthalmology*. 2012;119:2282–2289.
32. Ho J, Witkin AJ, Liu J, et al. Documentation of intraretinal retinal pigment epithelium migration via high-speed ultrahigh-resolution optical coherence tomography. *Ophthalmology*. 2011;118:687–693.
33. Domalpally A, Agrón E, Pak JW, et al. Prevalence, risk, and genetic association of reticular pseudodrusen in age-related macular degeneration: age-related eye disease study 2 report 21. *Ophthalmology*. 2019;126:1659–1666.
34. Steinberg JS, Fleckenstein M, Holz FG, Schmitz-Valckenberg S. Foveal sparing of reticular drusen in eyes with early and intermediate age-related macular degeneration. *Invest Ophthalmol Vis Sci*. 2015;56:4267–4274.
35. Querques G, Srour M, Massamba N, et al. Reticular pseudodrusen. *Ophthalmology*. 2013;120:872–872.e4.
36. Steinberg JS, Göbel AP, Fleckenstein M, et al. Reticular drusen in eyes with high-risk characteristics for progression to late-stage age-related macular degeneration. *Br J Ophthalmol*. 2015;99:1289–1294.
37. Waldstein SM, Vogl WD, Bogunovic H, et al. Characterization of drusen and hyperreflective foci as biomarkers for disease progression in age-related macular degeneration using artificial intelligence in optical coherence tomography. *JAMA Ophthalmol*. 2020;138:740–747.
38. Pollreisz A, Reiter GS, Bogunovic H, et al. Topographic distribution and progression of soft drusen volume in age-related macular degeneration implicate neurobiology of fovea. *Invest Ophthalmol Vis Sci*. 2021;62:26.
39. Wu Z, Luu CD, Ayton LN, et al. Optical coherence tomography-defined changes preceding the development of drusen-associated atrophy in age-related macular degeneration. *Ophthalmology*. 2014;121:2415–2422.
40. Jhingan M, Singh SR, Samanta A, et al. Drusen ooze: predictor for progression of dry age-related macular degeneration. *Graefes Arch Clin Exp Ophthalmol*. 2021;259:2687–2694.